Prospects on production technologies and manufacturing cost of oxide-based all-solid-state lithium batteries

Joscha Schnell,*[a] Frank Tietz, [b,c] Célestine Singer, [a] Andreas Hofer, [a] Nicolas Billot, [a] and Gunther Reinhart [a]

All-solid-state batteries (ASSBs) based on oxide solid electrolytes are promising future candidates for safer batteries with high energy density. In order to estimate the future manufacturing cost for oxide based ASSBs, a systematic identification and evaluation of technologies in solid oxide fuel cell (SOFC) and multi-layer ceramic capacitor (MLCC) production has been carried out. Based on a requirements analysis, these technologies are assessed towards their applicability in the production of ASSBs. The most promising technologies are compared by technology readiness using Monte-Carlo simulations. The comprehensive overview and systematic analysis of production scenarios for oxide-based ASSBs reveals significant advantages of established wet coating technologies, such as tape casting and screen printing. However, emerging technologies, such as the aerosol deposition method, could render the high temperature sintering step void. By comparison with SOFC production and adopting learning rates from conventional battery production, an estimation for the manufacturing cost of a garnet-based ASSB is given, indicating that prices below 150 $/kWh on cell level (incl. housing) are conceivable if material cost for the garnet solid electrolyte can be pushed below 60 $/kg. Based on these findings, scenarios for the scale-up from laboratory research to industrial scale can be derived, paving the way to mass production of safer batteries with high energy density.

Introduction

Lithium-ion batteries (LIBs) are the key for reliable energy supply and emission-free mobility. However, with increasing demand for higher energy densities, safety concerns arise[1], leading to costly efforts for safety management. Replacing the flammable liquid electrolyte by a non-flammable solid-state electrolyte (SSE) could reduce many of the risks associated with conventional LIBs[2]. However, polymer-based electrolytes suffer from low ionic conductivities at reasonable temperatures[3] and highly conductive sulfide-based SSEs have to be processed in inert atmosphere due to their reactivity with ambient air to avoid harmful H_2S formation[4]. In contrast, due to absence of flammable or toxic materials, all-solid-state batteries (ASSBs) using oxide ceramics offer the potential for safer energy storage applicable over a wide range of operating temperatures[5].

To be competitive with LIBs in terms of specific energy and energy density, Li metal needs to be integrated into ASSBs[6,7]. Therefore, dense SSE layers are required to inhibit dendrite growth, although creeping along grain boundaries remains an issue yet to be solved[8,9]. Sintering temperatures as high as 1250 °C are required to achieve room temperature ionic conductivities exceeding 10^{-4} S/cm[10,11], which is a prerequisite for application in electric vehicles[12]. Limited ion transfer at the interfaces between SSE and the electrode active materials will make the application of interlayers or co-sintering of the materials necessary[13]. Hence, new production technologies will be required compared to conventional lithium-ion cell production[14,15] (Table 1), necessitating a profound estimation of the resulting manufacturing cost.

The scope of this paper is, therefore, the systematic identification and evaluation of production technologies for oxide-based ASSBs, using methods developed in strategic technology planning. Different ceramic processing technologies are analyzed concerning their applicability for the production of SSE and cathode composite layers. The identified technologies are preselected based on their technical suitability and evaluated concerning the technology readiness, which serves to compare the most promising scenarios and to identify further development needs. Finally, based on the fabrication of solid oxide fuel cells (SOFCs), a top-down calculation of the manufacturing cost for different scenarios of large-format ASSBs with garnet SSE is presented. The results indicate that manufacturing cost can become competitive to conventional LIBs by economies of scale if ASSBs with high active material loadings can be fabricated.

[a] *Institute for Machine Tools and Industrial Management, Technical University of Munich, Boltzmannstraße 15, D-85748 Garching, Germany*
[b] *Forschungszentrum Jülich GmbH, Institute of Energy and Climate Research, Materials Synthesis and Processing (IEK-1), D-52425 Jülich, Germany*
[c] *Helmholtz-Institute Münster, Forschungszentrum Jülich GmbH, D-52425 Jülich, Germany*
* corresponding author
Electronic Supplementary Information (ESI) available: [details of any supplementary information available should be included here]. See DOI: 10.1039/x0xx00000x

Table 1: Comparison of various aspects during manufacturing and operation of ASSBs with different types of SSEs.

	Solid polymers	Sulfides	Oxides
Combination with Li metal anode	Stable against metallic Li[16]	Thermodynamic instability make protective layers or SEIs mandatory[17]	Several materials need a protective layer or SEI to avoid reduction by Li[17]
Mechanical properties	Elasticity very advantageous for wrapped designs	High conductivity allows thick layers for better robustness[18], ductility advantageous for densification[19], battery pack has to be permanently pressed	Brittleness may lead to cracking[20] and limit shaping to planar or tubular designs
Economic issues		All production steps have to be performed in inert gas[4], sintering step only necessary for hard materials	Sintering process has high impact on energy demand and costs[21]
Performance	Show limited rate capability[3]	Internal resistance has to be minimized by thin SSE layers and optimized microstructure of electrodes	Internal resistance has to be minimized by thin SSE layers and optimized microstructure of electrodes
Possible production technologies	Liquid processing, injection molding, extrusion, calendering	Pressing, wet coating, calendering	Ceramic processing technology, investigated in this paper

Requirements and properties of all-solid-state batteries

General remarks on solid-state electrolytes

General requirements for ASSBs, especially with regard to electric vehicle application, are high energy density, high power density, long life time, safety, and low cost[22]. Regarding energy density, a high content of active material in the ASSB is desirable, which calls for thick electrodes and thin SSE layers. Theoretical considerations concerning energy density and layer thicknesses can be found, e.g. in Placke et al. (2017)[7]. High power density implies fast ionic conductivity in electrodes and solid electrolyte layers, as well as sufficient electronic conductivity in the electrodes. Therefore, composite electrodes composed of active materials, SSEs and conductive agents are required[6], especially concerning the generally thicker cathode[7]. With regard to lifetime, the volumetric expansion and shrinkage of active materials during charge and discharge has to be taken into account[20]. Therefore, the use of low-strain active materials, such as $LiNi_{0.5}Mn_{1.5}O_4$ (LNMO)[23], or the integration of suitable binders is recommended[24]. Furthermore, the impenetrability and stability of the SSE layer plays an important role considering lifetime and safety of the ASSB. Costs are mainly governed by raw and processed materials, as well as the manufacturing processes for ASSB fabrication[15,21].

There are three types of solid-state electrolytes (SSEs) of relevance which can be grouped into sulfides, oxides, and polymers. A selection of the most reasonable SSEs is given in Figure 1 (image a). Here, the group of sulfides and oxides also include the thiophosphates and phosphates, respectively. The ionic conductivity at room temperature vary between 2 and 27 mS cm^{-1} for sulfides, 0.25 and 1 mS cm^{-1} for oxides, and 0.01 and 0.15 mS cm^{-1} for polymers, respectively. In comparison to liquid electrolytes having an ionic conductivity of 5 to 20 mS cm^{-1},[25] the sulfides can easily compete, whereas oxides have to be tailored properly in thickness and polymers do not seem to fulfill the conductivity threshold. Despite this low conductivity, first commercial ASSBs with solid polymers have been integrated into electric vehicles and have been produced by few companies[26,27]. For increasing the ionic conductivity and decreasing the internal resistance of these cells, the batteries are operated between 50 and 80 °C (see Figure 1, image a).

The question how thick a membrane of a dense SSE should be, can be answered according to former considerations used for the design of SOFCs. Here, the area-specific resistance (R_A) of a layered system has been used to target a specific internal resistance of the cell[28]. The area-specific resistance of a single component can be written as

$$R_A = L/\sigma \quad (1)$$

with L = thickness of the component and σ = conductivity. Imagining a 25 µm thick film of liquid electrolyte with σ = 20 mS cm^{-1} results in an R_A value of 0.125 Ω cm^2. However, the application of a porous separator in LIBs increases this value to 3.75 Ω cm^2 [29] due to the tortuosity of the membrane[30]. Since the cationic conductivity is only a fraction of the total conductivity, an even higher area-specific resistance can be assumed. For achieving the just mentioned value with a targeted 10 µm thick SSE, this membrane should have an ionic conductivity of 0.27 mS cm^{-1} (long horizontal gray line on the right side of Figure 1). Accordingly, an SSE with one order of magnitude higher and lower conductivity has to be one order of magnitude thicker and thinner, respectively. Since layers thicker than 10 µm are easier to produce and more robust during operation, the sulfides have a clear advantage over the two other classes of materials. However, the main drawbacks of sulfides are their limited thermodynamic stability[17], their strong sensitivity against air and moisture[4], the narrow potential window when elements like Ge and Sn are involved. Additionally, the high cost of Ge will exclude such compositions from commercialization. In general, oxides or sulfides with transition metal ions like Ti, Nb etc. or higher main group elements like Ga, Ge, Sn or others are prone to reduction when they are directly attached to metallic Li, leading to electronic conductivity and/or decomposition. Therefore, in such cases, a protective layer is necessary or other anode materials have to be used. In contrast, oxide SSEs with a garnet structure, such as LLZ, do not show any reaction up to 8 V in cyclovoltammo-grams[31] and seem to be stable against metallic lithium. However, first cell tests have shown that the ceramic separators are prone to reduction along grain boundaries[8] and recent research indicates limited stability against cathode potentials[17,32,33]. Due to the lower ionic conductivity compared to sulfide based SSEs, the thickness of the SSE layer and the microstructure of the electrodes need to be properly tailored to meet performance requirements. An overview of design concepts to meet these requirements will be given in the next section.

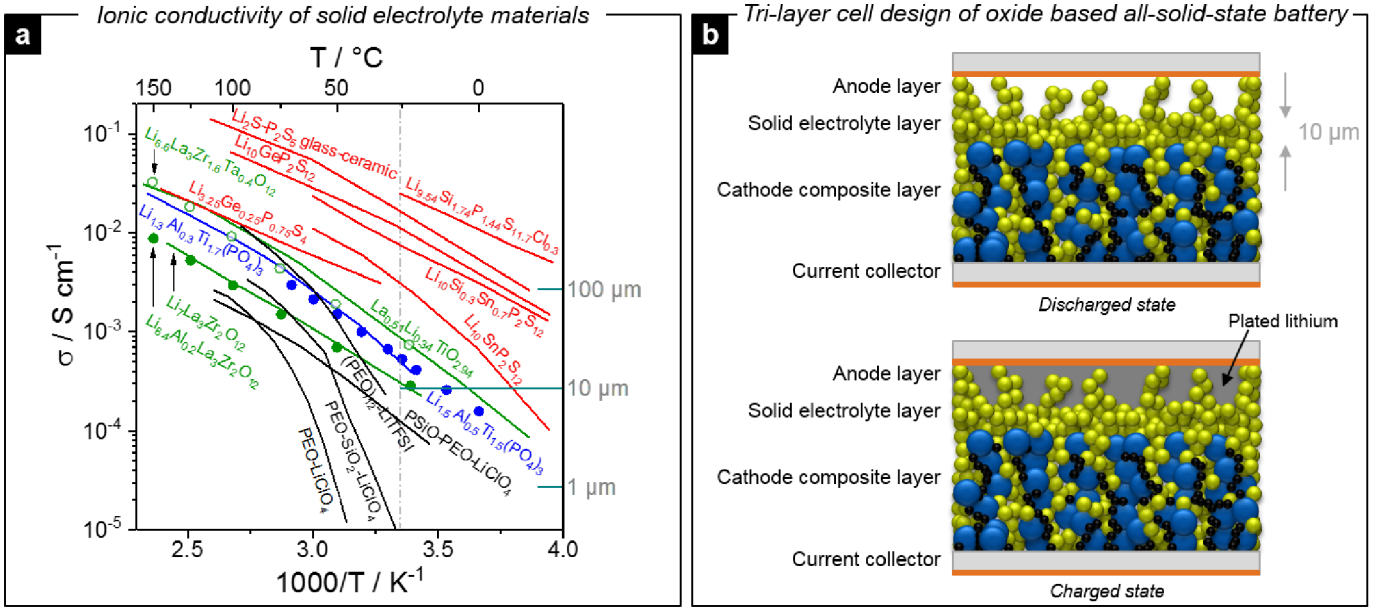

Figure 1: Comparison of the ionic conductivity of various SSEs (a) and possible cell design for an oxide based ASSB (b). Image a, red: sulfides and thiophosphates (Li$_{10}$GeP$_2$S$_{12}$ [34], Li$_{3.25}$Ge$_{0.25}$P$_{0.75}$S$_4$ [35], Li$_{10}$SnP$_2$O$_{12}$ [36], Li$_{10}$Si$_{0.3}$Sn$_{0.7}$P$_2$O$_{12}$ [37], Li$_{9.54}$Si$_{1.74}$P$_{1.44}$S$_{11.7}$Cl$_{0.3}$ [38], Li$_2$S-P$_2$S$_5$ glass ceramic [39]), green: oxides (Li$_7$La$_3$Zr$_2$O$_{12}$ (continuous line) [40], Li$_{6.6}$La$_3$Zr$_{1.6}$Ta$_{0.4}$O$_{12}$ (open circles)[8], Li$_{6.4}$Al$_{0.2}$La$_3$Zr$_2$O$_{12}$ (filled circles)[31], La$_{0.51}$Li$_{0.34}$TiO$_{2.94}$ (continuous line)[41]), blue: phosphates (Li$_{1.3}$Al$_{0.3}$Ti$_{1.7}$(PO$_4$)$_3$ (continuous line)[42], Li$_{1.5}$Al$_{0.5}$Ti$_{1.5}$(PO$_4$)$_3$ (filled circles)[43]), black: polymers (PEO-LiClO$_4$ [44], (PEO)$_{12}$-LiTFSI [45], PEO-SiO$_2$-LiClO$_4$ [46], PSiO-PEO-LiClO$_4$ [44]). The horizontal gray lines indicated with 1, 10 and 100 µm correspond to an area-specific resistance of 3.75 Ω cm^2 of the electrolyte layer (see text). Image b: Tri-layer cell[47] with dense garnet separator layer and porous garnet scaffolding (yellow spheres), cathode active material (large blue spheres) and conductive agent (small black spheres) infiltrated, and lithium anode (dark gray area) plated during the first charge.

Oxide-based all-solid-state batteries

Several types of ASSBs have already been proposed. For ductile sulfidic solid electrolytes, wet chemical processing and/or pressing of all cell components already leads to low porosities[19] and a good contact between the electrode and SSE particles[48], also enabling fast cycling[38]. However, for hard oxide-based SSE particles, simple pressing will not be sufficient to achieve layers with low porosity and sufficient ionic conductivity[19]. Therefore, other methods to achieve sufficient interfacial contact and low porosities are required.

One example is a patent application related to sodium batteries[49], but a similar concept and manufacturing route can also be realized for the lithium analogue. In this very generic concept, the cell is composed of a composite cathode (cathode active material and SSE), a phosphate-based solid electrolyte and a metallic anode. The proposed manufacturing of the cell is very similar to the processing of SOFCs, in which the cathode serves

as a substrate of the other cell components[50]. Similar to fuel cell production, the assembly of the cathode and electrolyte shall be realized by a single sintering step ("co-sintering"). However, during the recent years it has been demonstrated that most of the cathode materials react with the SSE at the high sintering temperatures required to densify the solid electrolyte, leading to undesired multiphase sintering products[51–53]. For instance, LNMO and LLZ have been shown to decompose at 600 °C[(52)], while a more recent publication indicated that co-sintering of $LiNi_{0.6}Co_{0.2}Mn_{0.2}O_2$ and LLZ up to a temperature of 700 °C may be possible[54]. However, temperatures higher than 1000 °C are required to achieve sufficient conductivity and density of the SSE layer[55].

Therefore, high-temperature sintering of the SSE layer needs to take place before adding the electrode active materials. Free-standing LLZ layers with dimensions of 2 x 2 cm² and thickness below 30 µm have been successfully prepared by suspension casting, green sheet pressing and sintering at 1090 °C for 1 h.[55] However, upscaling of these thin layers to large formats (> 10 x 10 cm²) and subsequent damage-free joining with a cathode composite (70 µm to 150 µm thickness[15]) will turn out to be challenging.

In order to overcome these issues, a different battery design ("tri-layer cell") has been proposed, consisting of two porous SSE layers and a dense SSE layer made of a garnet-type material[47], as schematically depicted in Figure 1 (image b). The thick and porous outer layers are sintered at high temperatures (>1000 °C) and serve as scaffolds for the infiltration or impregnation of active materials. Also this approach has been very well known from SOFC development[56,57]. It offers several advantages, such as adjustable pore size and volume for flexible use of active materials. The inventors reported a cell structure with a 25-30 µm thick SSE layer and two porous layers with a thickness of 50 µm each[58], while more recently, a SSE layer with 14 µm thickness and 70 µm thick outer porous layers was presented[59]. Using a three-point bending test, the authors report a highly increased mechanical strength of the tri-layer design compared to a single, free-standing membrane[59]. A different approach to obtain 3D-structures in the cell can be achieved with patterned or so-called hole-array electrolyte layers, for example by punching with a specially designed die with patterned structure[60]. Another option could also be structuring by laser ablation, which has successfully been applied for conventional LIB electrodes[61].

Moreover, a processing route known from thin-film ASSBs seems to be plausible. Here, instead of high temperature sintering, a dense SSE layer is fabricated by vapor deposition[62] or aerosol deposition methods[63,64].

Results and discussion

Technology screening: Ceramic processing technologies

In order to provide competitive energy and power densities at reasonable cost, precise tuning of layer composition and thicknesses as well as implementation of scalable production processes will be required[15]. However, in contrast to conventional lithium-ion cells, the brittleness and resulting fragility of the materials will impose new challenges for mass production[15]. For technology screening (cf. methods section), two major fields of interests were prioritized to identify manufacturing technologies potentially applicable to ASSB production:

The SOFC is an energy conversion system using an yttria-stabilized zirconium dioxide ceramic layer as separator. An SOFC can be manufactured in tubular as well as planar design. A planar cell can be built up in three different types: electrolyte, cathode or anode-supported, each component can act as substrate layer to carry the cell. The first step to fabricate an electrolyte-supported SOFC is the preparation of the electrolyte slurry using a solvent-based mixing process. This mixture is then applied onto a carrier foil, e.g. by tape casting, and dried to produce the solvent-free "green tape". After removing the carrier foil, a cutting process is necessary before sintering the green tape at elevated temperatures to obtain near-net-shape components. The electrodes are subsequently coated onto the electrolyte layer in a similar fashion, e.g. by screen printing[65]. Usually the electrodes are sintered separately at different temperatures due to varying sintering properties of anode and cathode materials. However, in the ideal case only one sintering step densifies the complete cell. The fabrication of a cathode or anode-supported SOFC is similar to the processes described for the electrolyte-supported SOFC. A key difference between these two technology chains is the number of sintering steps: Also here the ideal and more sophisticated production process involves only one co-sintering sintering step of electrode and electrolyte to obtain an electrode-supported half-cell[66] and a second sintering step of the other electrode. In practice, however, up to four thermal treatments can become necessary[50,67] when the starting materials do not have matching sintering behavior: 1) pre-sintering of the electrode substrate, 2) co-sintering of electrode substrate, additional electrode layer and electrolyte layer, 3) sintering of a diffusion barrier layer (if necessary) and 4) sintering of the second electrode layer.

Similar to the SOFC, the fabrication of multi-layer ceramic capacitors (MLCC) is a potential field of interest, because the dielectric device consists of a solid oxide ceramic layer, e.g. $BaTiO_3$. Processing methods for MLCCs have already been implemented in commercial mass production. Therefore, technologies used in MLCC fabrication are also relevant for the scouting of manufacturing processes for ASSBs. The technology chain of a MLCC also starts with the preparation of the ceramic slurry for the dielectric which is then applied on a carrier foil, e.g. by tape casting. After drying and cutting the tape, the electrodes are applied, e.g. by screen printing. Further technologies involve the stacking, lamination, sintering, and termination of the MLCC before final packaging[68].

Evaluation of production technologies

The layer fabrication processes in particular can be regarded as so-called core technologies[69], since these are the process steps which mainly define and influence the required upstream and downstream technologies. An overview of the identified layer fabrication technologies is given in Table 2. These technologies

were analyzed concerning the technical suitability to fabricate SSE and cathode composite layers (cf. methods section). On the basis of the earlier defined exclusion criteria, most vapor-based coating technologies were eliminated because of the high error rate for fabrication of a 5-30 µm thick SSE layer or a 70-150 µm thick cathode composite layer with dimensions > 5 x 5 mm². Most plasma- or flame-based spraying technologies were excluded because of the limited thermal stability of the materials during processing[70]. Therefore, only six and eight technologies were considered for further evaluation for SSE layer and cathode composite fabrication, respectively (cf. Table 2). For rough evaluation of the technical feasibility, the degree of fulfilment for material, product and production related criteria was evaluated and depicted in a suitability diagram, as illustrated in Figure 2 (images a and b): For layer fabrication, material related criteria comprise the chemical and thermal stability of the coating materials and the substrate. Product related criteria are the feasibility to generate the desired layer thicknesses and geometries at a low error rate, as well as the resulting density of the fabricated layer. Production related aspects are throughput, e.g. deposition rate, as well as environmental considerations, such as vacuum, processing gas or high energy consumption (cf. Supplementary Tables S2 and S4).

Technology chains

Two exemplary process chains were derived from the above presented results, as depicted in Figure 3. Figure 3 (image a) illustrates the fabrication of a cathode-supported half-cell where the solid electrolyte layer is applied after slurry mixing, tape casting, low-temperature sintering, and shaping of the cathode composite layer. An aerosol deposition step is used for fabrication of the SSE layer, since a high layer quality and density can be achieved without a high temperature co-sintering step and the resulting unwanted side reactions. A subsequent tempering step (approx. 600 °C) is applied for thermal curing[64]. The lithium metal anode and current collector(s) are joined before cell assembly and packaging. The advantage of this processing route is the omission of high-temperature sintering steps and the possibility to combine different solid electrolyte materials for cathode composite (e.g. LATP) and solid electrolyte layer (e.g. LLZ)[71]. Here, the overall technology readiness of the technology chain for fabrication of the cathode-supported cell is dominated by the low maturity level of the aerosol deposition step

In Figure 3 (image b), the process chain of a tri-layer SSE matrix is described, with three subsequent tape casting processes to produce the scaffolding, as described in a recent publication by Hitz *et al.*[59]. These layers can be fabricated as individual green sheets which are subsequently laminated on top of each other[59]. Another possibility would be to directly cast the layers on top of each other after each solvent evaporation step. The porosities of the outer layers can be tuned by using appropriate slurry mixtures (i.e., addition of pore formers)[59]. This is vital for the later infiltration of the active materials[72,73] and to achieve a high surface area to enable large-current densities[59]. The green tapes are subsequently cut to size before the high-temperature sintering step in which the pore formers in the outer layers are removed. By carefully tuning the particle size and sintering parameters[55], a dense (> 99 %) SSE layer between the two porous layers can be achieved which is able to efficiently suppress lithium dendrites during battery operation[59]. Quality control after sintering will be indispensable in order to detect defects such as pinholes or cracks, e.g., by means of a quality gate[74]. To hinder degradation of LLZ due to humidity and Li_2CO_3 formation, further processing after sintering should take place in dry or inert atmosphere[75].

The cathode slurry is infiltrated into the upper porous structure using a screen printing process. Note that this process may have to be repeated several times to fill up the porosities remaining after solvent evaporation[72]. Smaller cathode particles seem to be beneficial to achieve a denser particle arrangement and to buffer volume changes of the active materials during battery operation[54]. Fine tuning of slurry viscosity and solids content will be required to achieve proper filling of all pores. The cathode infiltration is followed by sintering at lower temperature to ensure mechanical and ionic contact between SSE matrix and cathode particles. A low temperature melting glass, such as Li_3BO_3 can be added to the cathode slurry to reduce sintering temperatures[13,54]. Subsequently, the anode is infiltrated into the other porous layer of the scaffolding, for instance by melt processing[73]. Since molten lithium is very reactive, safety precautions and inert processing atmosphere are indispensable. A surface treatment can be applied to enhance wettability of the lithium[76] and to form a mixed-conducting network[77]. During infiltration, particular care must be taken not to cause an external short circuit.

Finally, the current collector(s) are joined and the cell is assembled. Although the tri-layer setup leads to higher mechanical strength than free-standing layers[59], handling of the fragile ceramic layers during mass production using fully automated equipment will be a challenge. Hence, elaborate design of gripping principles, especially during cell stacking will be required, similar to the handling of ultrathin glass or crystalline wafers in the semiconductor, photovoltaics, or optoelectronics industries. For both illustrated concepts (cathode supported or tri-layer design), fine tuning of the process parameters during layer fabrication and sintering is a prerequisite for functional ASSBs.

Table 2: Overview of different layer fabrication technologies applied in ceramics processing and suitability for SSE and cathode composite fabrication.

Material input	Processing technology	Thickness range	Substrate requirements	Temperature of coating material	Temperature of substrate during coating	Industrial field of application	Ref.	Suitable for SSE	Suitable for cathode	Exclusion criteria
Suspension	Tape casting	10-800 µm	Flexible	-	-	Ceramic industry	[66,78,79]	X	X	
	Slip casting	1-20 µm	Open porosity	-	-	SOFC	[78]	X	X	
	Extrusion	>200 µm	-	-	-	Ceramic industry; construction industry	[78]		X	Error rate
	Screen printing	5-100 µm	Planar, even	-	-	Ceramic industry; micro technology	[78,80]	X	X	
	Roller coating	5-50 µm	Planar, even	-	-	Ceramic industry	[78,81]	X	X	
	Dip coating	2-10 µm	Porous, high surface quality	-	-	Ceramic industry; electronics	[78]			Error rate
	Wet powder spraying	5-100 µm	-	-	-	Automobile; white goods; electronics	[78,81]		X	Error rate
	Electrophoretic deposition (EPD)	>1 µm	Electrically conducting	-	-	Lab scale for SOFC; biology; medicine; automobile	[79,82,83]	X	X	
Gas phase	Chemical vapor deposition (CVD)	1-10 µm/h	Porous, thermally stable	150 °C	400-1200 °C	Microelectronics	[78,79,84]			Thermal stability, error rate
	Electrochemical vapor deposition (EVD)	2.8-52 µm/h	Porous, thermally stable	150 °C	400-1200 °C	Microelectronics	[84,85]			Thermal stability, error rate

	Physical vapor deposition (PVD)	0.5-2.5 µm/h	Thermally stable	350 °C	70-400 °C	SOFC; aviation industry	[78,84,86]			Thermal stability, error rate
	Pulsed Laser Deposition (PLD)	0.15-0.5 µm/h	Thermally stable	500-700 °C	500-700 °C	Ceramic industry; material science	[84]			Error rate
Sprayed powder	Aerosol deposition method (ADM)	1-100 µm	-	25 °C	25 °C (200-300 °C during impact)	Ceramic industry; material science	[87–90]	X	X	
	Atmospheric plasma spraying (APS)	40-300 µm	Thermally stable, high surface hardness	>4500 °C	100-300 °C	Ceramic industry, turbine industry	[78,91,92]			Thermal stability
	Vacuum plasma spraying (VPS)	30-150 µm	Thermally stable, high surface hardness	>5000 °C		Ceramic industry	[78,92,93]			Thermal stability
	Very low-pressure plasma spraying (VLPPS)	20-100 µm	Thermally stable	>4700 °C		Ceramic industry; aviation industry	[78,91,94]			Thermal stability
	Flame spraying	80 - 150 µm	Thermally stable	>2700 °C	>300 °C	Material science; corrosion protection	[78,81,84,92]			Thermal stability
	High-velocity oxy-fuel spraying (HVOF)	5-50 µm	Thermally stable, high surface hardness	>1000 °C		SOFC; ceramic industry	[78,92,95]			Thermal stability

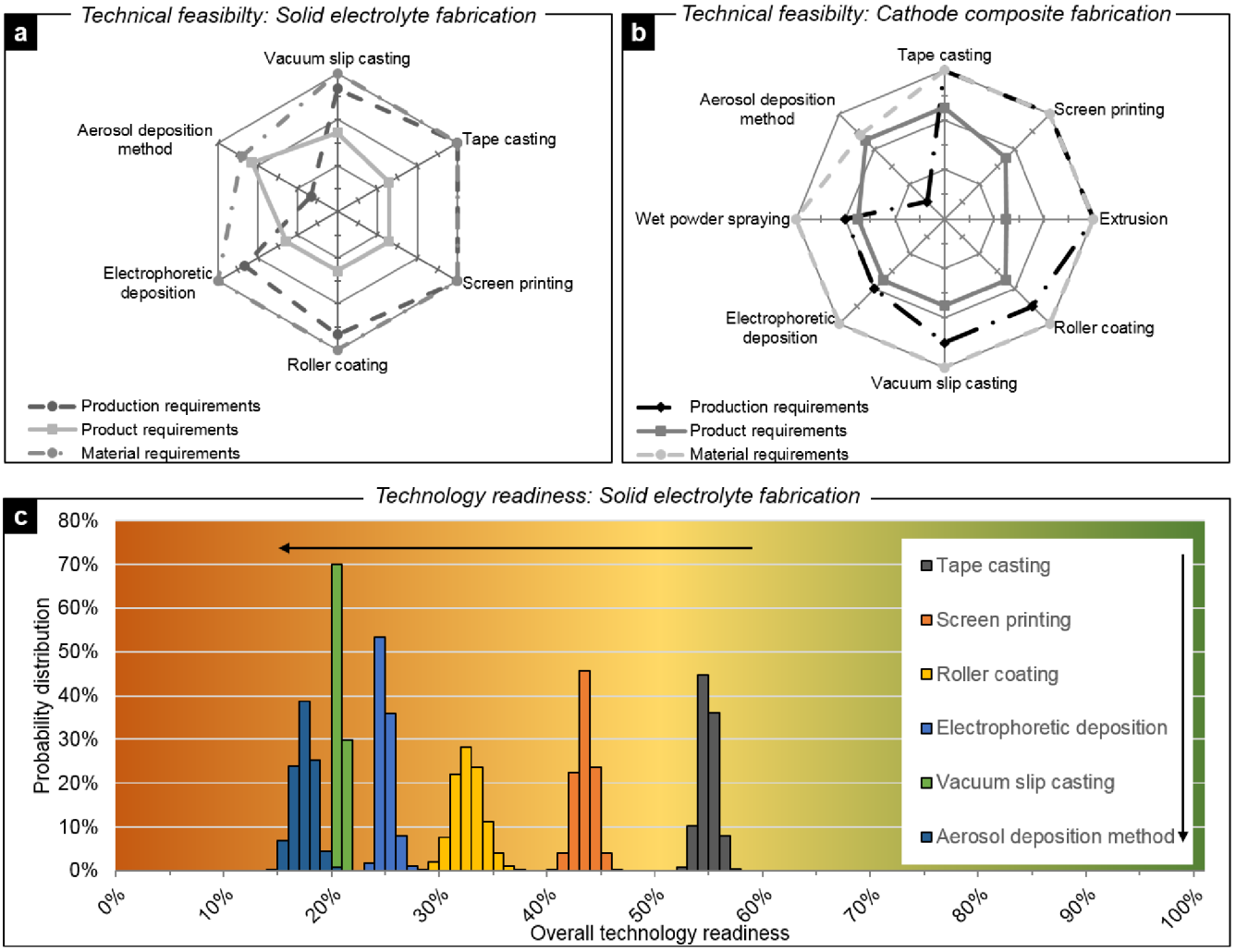

Figure 2: Evaluation of production technologies for ceramic layer fabrication. Comparison of technologies with regard to technical feasibility for solid electrolyte separator fabrication (image a) and cathode composite fabrication (image b), as well as technology readiness based on a Monte-Carlo Simulation for solid electrolyte separator fabrication (image c). The arrows in image c assign the technologies (from Tape Casting to Aerosol Deposition) to the respective histograms (from right to left).

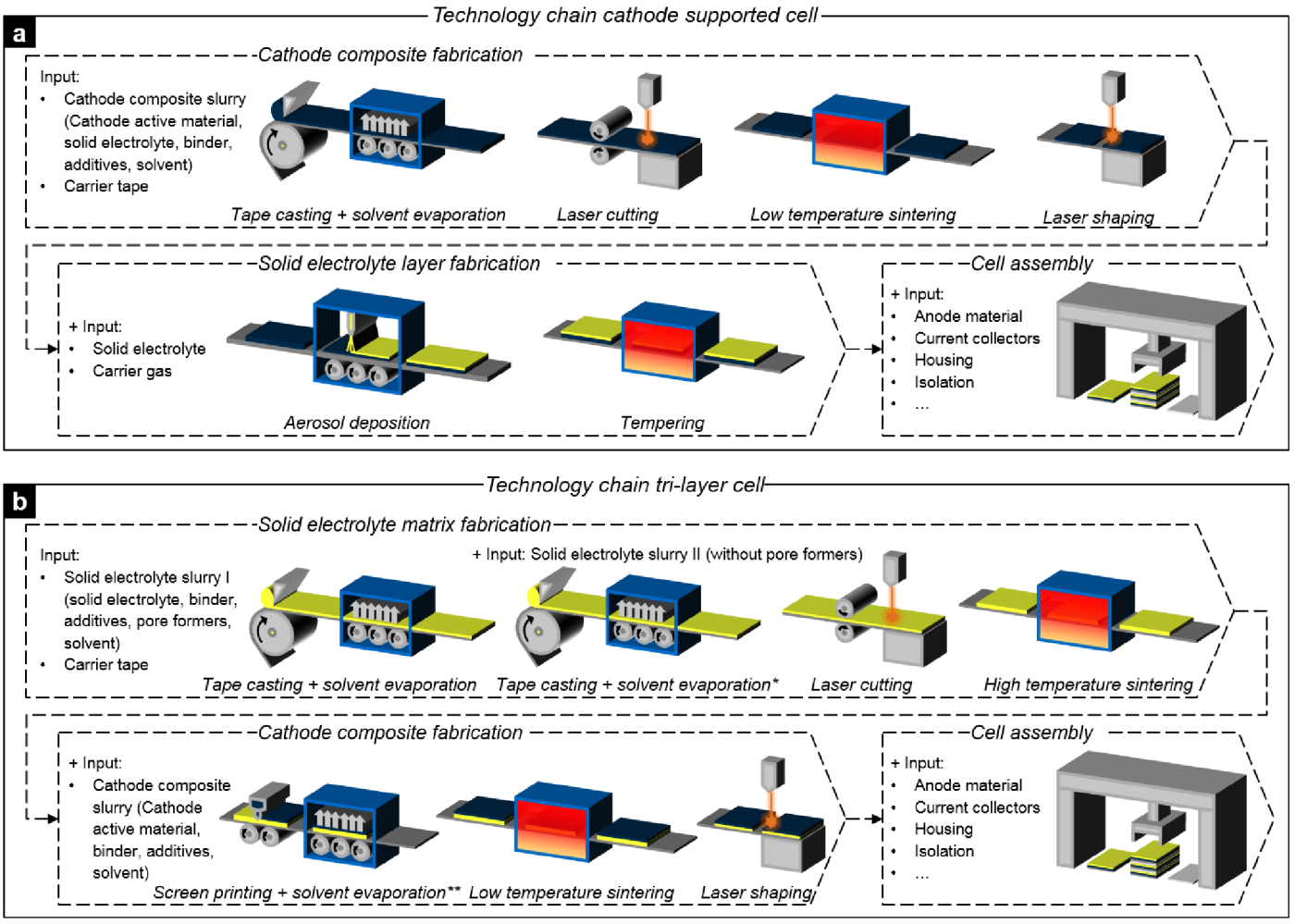

*Figure 3: Exemplary technology chains for cathode-supported cell (a) and tri-layer cell (b). *The layers are either coated on top of each other, or fabricated as individual green sheets and subsequently laminated. This process step can be repeated with solid electrolyte slurry I for the anode side if required. **This process step can be repeated several times to account for shrinkage during solvent evaporation in order to fill all remaining pores.*

Production cost estimation

While the low maturity level of the aerosol deposition process currently rules out a reasonable cost estimation, a first approach was made to approximate the manufacturing costs of the tri-layer ASSB by identifying a reference technology chain. Because of the similarities to the fabrication of solid oxide fuel cells (SOFCs), the process chain of an electrolyte-supported SOFC manufactured in small scale production (several 10,000 cells per year) by the company Kerafol is used as reference (cf. methods section). As illustrated in Figure 4 (image a), the total production costs sum up to 20 $/SOFC, where processing cost (personnel cost, high temperature sintering, and further manufacturing cost, such as plant depreciation) corresponds to 75 % and material cost corresponds to the remaining 25 %.

As shown in the previous section, processing of a tri-layer oxide-based ASSB consists of similar process steps, although the required sintering temperatures for the SSE layer and the heat treatment to compact the cathode in the electrolyte framework are expected to be lower for ASSB production[10,13]. Processing cost were assumed to be comparable to SOFC production, while material cost was calculated for an ASSB galvanic cell with similar dimensions (cf. methods section). Assumptions on the mate-

rial prices were taken from literature values[96–99] (cf. Supplementary Table S5), while the initial LLZ price was set to 2000 $/kg, based on numbers by the company *MSE Supplies LLC* (Ampcera™) for LLZ quantities above 100 kg. Since the literature values for the other components rather correspond to mass production scenarios, the LLZ price dominates the overall material cost, with a significant share corresponding to the LLZ in the cathode.

Since LLZ prices are expected to significantly decrease for higher production volumes, a scenario analysis was conducted. The LLZ price was set to 50 $/kg, and different scenarios for cathode material and cathode thickness were evaluated: For the base scenario (70 µm thick LNMO cathode), material costs add up to 0.12 $ per galvanic cell. In order to increase the overall energy density, the cathode thickness could be increased up to 150 µm assuming that ionic percolation is sufficiently high. Hence, also the anode thickness needs to be increased to account for the higher area specific capacity of 5.5 mAh/cm². This would result in a price of 0.23 $ per galvanic cell. A significant increase in energy density could be achieved if the cathode material was replaced by Li-rich $LiNi_{1-x-y}Mn_xCo_yO_2$ (HE-NMC)[100]. Here, a 70 µm thick cathode would result in the same areal capacity as for the 150 µm thick LNMO cathode, and a 150 µm thick cathode (11.5 mAh/cm²) would result in an energy density of up to 530 Wh/kg on galvanic cell level. Note that HE-NMC has a porous structure[101] which can hardly be infiltrated by solid electrolyte particles, so significant changes in materials properties will be required for these components to be compatible with each other.

In order to simulate a mass production scenario, processing costs were adapted to account for learning rates with increasing production volume. Learning rates in conventional LIB pack production for electric vehicles were estimated as 16±4 %, i.e. by doubling the cumulative production capacity, average prices decreased by approximately 16 %.[102] This value was used to estimate the processing cost in $/kWh for a bipolar stacked ASSB as a function of production volume, as illustrated in Figure 4, image b. Here, a prismatic HEV cell format (85 mm x 120 mm x 12.5 mm)[103] and a 1 mm thick aluminum housing (corresponding to 0.5 mm wall thickness) were assumed for further calculations. The numbers of galvanic cells was varied to account for the available space in the HEV cell housing, based on the respective cathode and anode layer thicknesses (cf. methods section). The colored areas in the double logarithmic plot correspond to varying cathode thicknesses (70 µm to 150 µm) for LNMO (red dotted lines) and HE-NMC (blue lines), where thicker cathodes result in lower prices per kWh due to the higher active material content. Processing costs decrease from approximately 750-2500 $/kWh for small scale production (10.000 HEV cells per year) down to 75-240 $/kWh for a cumulated production volume of 100 million produced HEV cells (cf. Table 3). Since the energy content of one HEV cell varies between 126.4 Wh (LNMO, 70 µm) and 171.6 Wh (HE-NMC, 150 µm), a production volume of 100 million produced cells corresponds to an annual output of approximately 10-20 GWh, similar to the current output of Tesla's Gigafactory[104]. The vertical bars in Figure 4 (image b) indicate the numbers of produced cells corresponding to a cumulated output of 10 GWh, which would suffice to equip 200.000 electric vehicles with a 50 kWh battery pack each. Hence, if production were running at full capacity, it would take roughly 1.5 to 2 years to achieve the cost reduction associated with a cumulated production of 100 million cells. Of course, this scenario presumes that an all-solid-state battery with competitive energy, power and cycle life can be reproducibly fabricated and transfer to pilot and industrial scale have been successfully achieved, which could take up many more years. As a guide for the eye, material cost (incl. hard case packaging) was also indicated at a constant LLZ price level of 50 $/kg, which is expected to be a realistic value for large production quantities. Adding up materials and processing cost would result in a total cost of 140-350 $/kWh.

Despite the optimistic learning rate scenario, processing costs still take up more than half of the total cost, even for mass production. This is rather uncommon for a complex product with cost intensive materials (such as a LIB), where material cost usually take up far more than half of the total product cost, up to 70-80 % for Li-ion cells[105,106]. Although the presented calculation can only serve as a rough estimate, this could be an indication for the high impact of the sintering step which accounts for 20 % of the processing cost. Note that these calculations already presume that with increasing production volume, the cost for sintering can be reduced in a similar fashion as the other processing costs. To illustrate the sensitivity of the model with regard to the learning rate, further estimations for different scenarios (learning rates of 12 % and 20 %, respectively) can be found in Table 3. Of course, also the cost and energy content of the cathode active material has a significant influence on the overall cell cost, which was already shown in calculations for conventional lithium-ion cells[97]. Therefore, it is important to aim for cathodes with a high energy density and a low Co content[22].

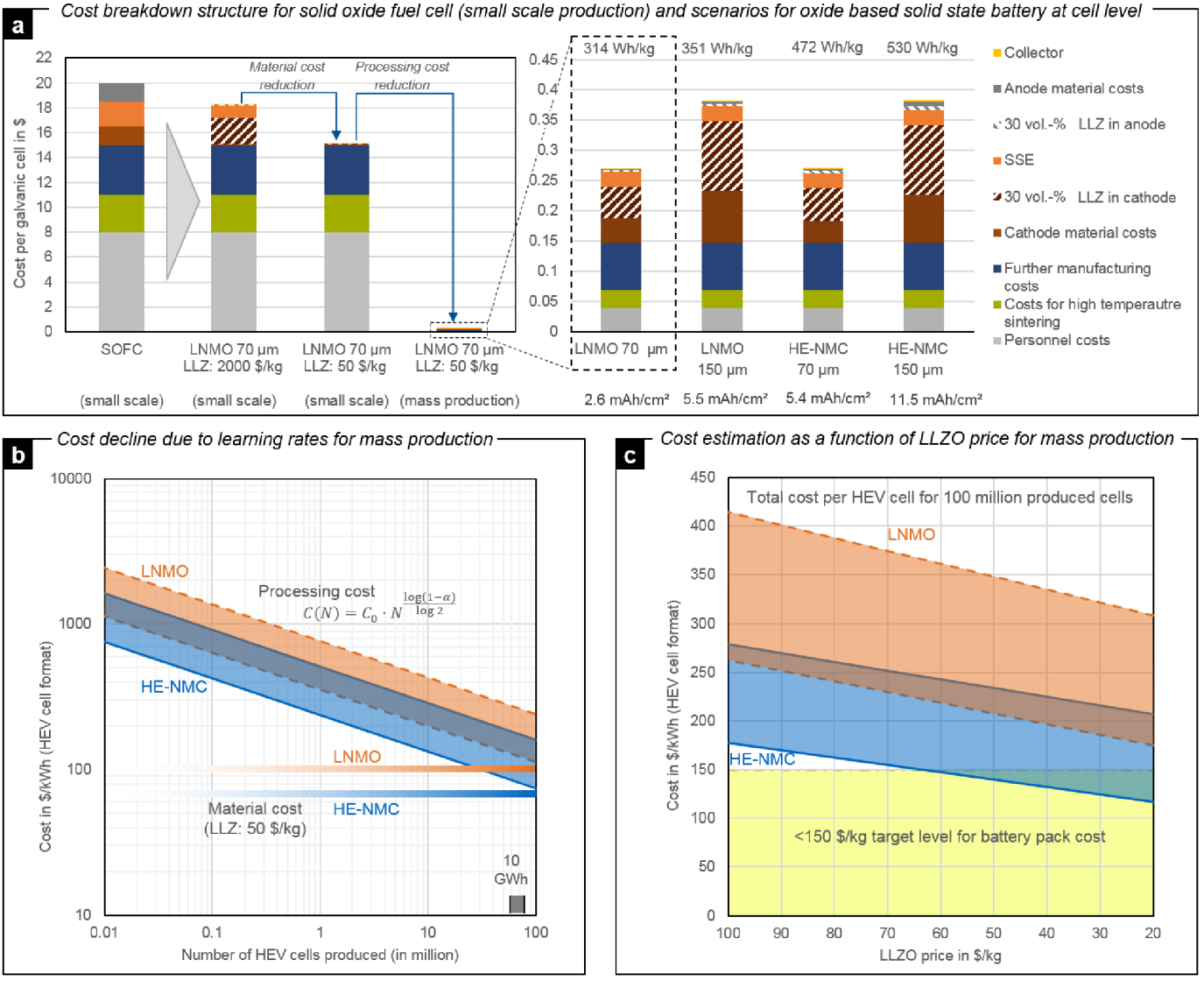

Figure 4: Procedure for manufacturing cost estimation for a tri-layer garnet based ASSB. Image a: Based on the cost breakdown structure for small scale production of a solid oxide fuel cell (SOFC), manufacturing cost for an ASSB was estimated. Processing cost (personnel cost, high temperature sintering, and further manufacturing cost) were assumed similar to SOFC production, whereas material cost were calculated for a 70 µm thick LNMO composite cathode (60 vol% active material, 30 vol% LLZ, 5 vol% carbon black, 5 vol% binder), a 10 µm thick LLZ separator layer, a composite anode (30 vol% LLZ 1:1.1 positive to negative ratio), and a 10 µm thick bipolar current collector (99 vol% Al; 1 vol% Cu). In a first step, the LLZ-price was reduced from 2000 $/kg to 50 $/kg. The inlay (right) shows the resulting material cost and different scenarios for cathode active material (LNMO, HE-NMC) and cathode thicknesses (70 µm and 150 µm) with resulting specific energy. In a second step, learning rates were adopted from conventional LIB pack production[102] to account for processing cost reduction with increased production volume up to a mass production scenario with 100 million produced cells (image b): Here, the processing cost for production of a bipolar stacked prismatic HEV cell (85 mm x 120 mm x 12.5 mm, aluminum housing with 0.5 mm wall thickness) was calculated as a function of production volume with learning rate α = 16 %. As a guide for the eye, material cost is also indicated (horizontal bars). The colored areas account for different cathode thicknesses (70 µm to 150 µm). Image c: Total cost (processing + material) for mass production of HEV cells as a function of LLZ price.

In Figure 4, image c, the total manufacturing cost (material cost and processing cost) for a mass production scenario (100 million produced cells, learning rate of 16 %) is depicted as a function of LLZ cost which was varied between 20 $/kg and 100 $/kg. The colored areas correspond to varying cathode thicknesses for LNMO (red dotted lines) and HE-NMC (blue lines) where thicker cathodes (150 µm) correspond to lower overall cost. The simulation reveals that if LLZ prices were pushed towards 20 $/kg, the cost per HEV cell (including hard case packaging) could fall below 180-310 $/kg for LNMO and even below 120-210 $/kg for HE-NMC. As indicated by the horizontal yellow dash-dotted line,

target cost on battery pack level (<150 $/kWh) in the automotive industry[107] can only be reached with a very optimistic configuration (150 µm thick HE-NMC). However, since the volume change in the anode has been considered in the calculations for cell design (no external pressing) and a complex cooling system will potentially not be needed for ASSBs, the cost increase from cell to module and pack level is expected to be lower than for conventional LIBs. Improvements on target cost could be achieved by reducing inactive material content, e.g. reduction of LLZ in anode and cathode. This would, however, lead to decreased rate capability. Another option could be to use a pouch bag instead of an aluminum hard case. Dimensions at HEV size reflect a challenging, yet realistic scenario for oxide based sintered ASSBs. Aiming for larger cell formats (plug-in hybrid electric vehicle, PHEV, or battery electric vehicle, BEV)[103] could further increase the energy density per cell and reduce manufacturing costs per kWh. However, as discussed above, the handling operations for automated processing will become increasingly difficult for layers with a larger area. From a production perspective, lower sintering temperatures and even larger production volumes would result in decreasing price levels.

Table 3: Specific energy densities and costs for different cell designs on galvanic cell level and stack level (incl. housing) for a mass production scenario (100 million produced cells, 50 $/kg LLZ) with different learning rates α. The values were calculated for bipolar stacked prismatic HEV cell (85 mm x 120 mm x 12.5 mm, aluminum housing with 0.5 mm wall thickness) with a composite cathode (60 vol% active material, 30 vol% LLZ, 5 vol% carbon black, 5 vol% binder), a 10 µm thick LLZ separator layer, a composite anode (30 vol% LLZ 1:1.1 positive to negative ratio), and a 10 µm thick bipolar current collector (99 vol% Al; 1 vol% Cu).

Galvanic cell level						**Stack level (incl. housing)**					
Cathode active material	Cathode thickness	Anode thickness (charged)	Specific energy	Material costs	Galvanic cells per stack	Energy per stack	Specific energy	Material costs	Total costs (α=12 %)	Total costs (α=16 %)	Total costs (α=20 %)
	µm	µm	Wh/kg	$/kWh		Wh	Wh/kg	$/kWh	$/kWh	$/kWh	$/kWh
LNMO	70	20.0	313.8	102.6	104	126.4	288.2	108.2	934.2	348.2	173.8
LNMO	150	42.9	351.9	90.7	54	140.7	323.0	95.7	481.2	207.7	126.4
NMC 811	70	30.6	363.3	92.5	95	138.7	332.2	97.6	785.2	297.3	152.2
NMC 811	150	65.5	405.6	82.6	48	150.2	369.8	87.3	408.2	188.2	112.8
HE-NMC	70	41.5	472.6	68.8	87	158.3	427.0	73.3	625.0	233.5	117.1
HE-NMC	150	88.9	530.2	60.9	44	171.6	477.5	65.0	322.4	139.8	85.4

Conclusions

The presented results reveal the dilemma that experimental research currently faces during scale-up of ASSB fabrication using oxide SSEs: While mature slurry-based technologies can provide dense layers with high throughput on a large scale, the required high sintering temperatures inhibit co-firing of SSE and cathode particles. Therefore, for cathode-supported ASSBs, vapor or aerosol deposition methods seem to be the only plausible option to generate SSE dense layers without high temperature sintering, limiting throughput to the layer growth rate. For the trilayer electrolyte matrix, a bottleneck in production can be the infiltration of the electrode materials into the outer, porous layers, which requires very fine tuning of the porosities and of the process parameters during infiltration and subsequent low temperature annealing. As indicated by the maturity assessment, manufacturing equipment readily available in the ceramics industries (e.g., SOFC or MLCC production) can potentially be adapted to the fabrication of oxide-based ASSBs. This can be a potential market opportunity for machine and equipment engineering and the ceramics industry, although processes such as surface treatment or infiltration of electrodes into porous structures can pose an issue yet to be solved for large-scale production. The results presented in this paper can help the respective stakeholders in up-scaling from research to pilot scale and identifying suitable technologies for focusing on development efforts. The systematic procedure for technology evaluation, derived from established methods in strategic technology planning, can assist to provide information on manufacturing technologies despite the early stage of development and the resulting uncertainty concerning product properties and production technologies. Although the top-down calculation for the manufacturing cost can only serve as a rough estimate and is highly sensitive to the assumed learning rate, the presented results indicate that garnet based ASSBs could be feasible by economies of scale despite the high temperature sintering step. However, as the calculation reveals, a prerequisite will be the fabrication of thin SSE layers and the integration of high energy electrode materials and high active material loading, which must be capable of stable cycling at sufficiently high current densities. Therefore, further material innovation and research will be required, especially with regard to the interfaces between SSEs and electrode materials[24] and the scale-up of cell dimensions and production processes[15].

In summary, a comprehensive and systematic evaluation of ceramic processing technologies with regard to large-scale production of ASSBs was demonstrated. Based on theoretical considerations concerning the properties of the respective SSEs, re-

quirements for layer fabrication were deduced and ceramic processing technologies were evaluated with regard to their suitability to meet these requirements. For fabrication of the SSE layer, the aerosol deposition was found to be most suitable, whereas for the cathode composite layer, tape casting and screen printing show the most promising results. The technology readiness evaluation revealed relatively high maturity level of the tape casting and screen printing processes, while the aerosol deposition method will require high development efforts to reach acceptable maturity levels for mass production. A cell cost estimation for different types of cathode active materials and layer thicknesses was conducted and reveals that garnet based ASSBs could be competitive with costs for conventional lithium-ion cells if the price for LLZ can be pushed below 60 $/kg or if lighter SSEs employed, e.g. in the cathode composite. While further experimental validation is required to manifest the presented findings, future research will have to focus on innovative layer densification technologies or new materials with low sintering temperatures. Furthermore, a bottom-up calculation of the processing cost, taking into account every single production step along the process chain, would enable a more detailed investigation on potential cost drivers in ASSB production. The results presented in this paper can assist researchers, (potential) cell and equipment manufacturers, and OEMs to make profound decisions in taking the next steps towards high-energy batteries with improved safety.

Methods

Technology identification and evaluation

A concept for the identification and evaluation of manufacturing technologies for ASSBs[14] was adapted from strategic technology planning methods[69,108,109] to the specific requirements of ASSB fabrication, as illustrated in Figure 5. The first step to identify suitable processing methods for commercial mass production of ASSBs is the determination of search fields for technology scouting[108]. Based on the different materials and components as well as the specific requirements of the ASSBs, promising search fields are energy systems containing ceramic layers, such as SOFCs and capacitors. Focusing on ceramic layers, requirements for the identified technologies are derived for cathode composite and SSE layer.

Based on a literature and patent search, different layer fabrication technologies were identified and the resulting technology profiles were stored in a database. Subsequently, a preselection of technologies was conducted based on the technical suitability. For this purpose, exclusion criteria were defined as suggested by Klocke et al. (2000)[69], with a focus on material compatibility and the main functionality of the product: Hence, the thermal stability of the coating and substrate materials (SSE, cathode materials) during processing was taken into account, as well as the error rate for the defined layer geometries during fabrication. Technologies not fulfilling these criteria were excluded from further consideration.

In a second step, a rough evaluation of the technology capability was conducted based on a workshop with three experts with more than 10, 20 and 25 years of experience in ceramics processing and involved in different technological fields (power plant and aircraft industry, electro-ceramics, energy technologies). The evaluation included the capability to meet product requirements, such as layer thicknesses, obtainable sizes of the components, consideration of material characteristics, and production-related aspects such as throughput. These criteria were weighted separately for the fabrication of SSE layer and cathode composite layer (Supplementary Tables S1 and S3). The weighting of the criteria was balanced by the experts by pairwise comparison. A decision matrix was used to collate the technology profiles with the weighted criteria, enabling a ranking using performance indicators M_{T_j} of the technologies based on technical suitability:

$$M_{T_j} = \frac{\sum_i^n w_i \cdot P_{i,j}}{\sum_i^n w_i},\ w_i \in \{1;2;3\},\ P_{i,j} \in \{0;1;2;3\} \quad (4)$$

Here, w_i is the (normalized) weighting of criterion i and $P_{i,j}$ is the degree of fulfillment for technology T_j with regard to criterion i on a scale from zero to three. For fabrication of the SSE layer, especially product requirements, such as layer density and error rate, were rated most critical. The final ranking was calculated by multiplying the weighted average of each technology in every category by the performance indicator M_{Tj}.

Using the decision matrices depicted in Supplementary Table S2 (SSE layer) and Supplementary Table S4 (cathode composite), the respective technologies were ranked according to their suitability to meet the aforementioned criteria. For graphical illustration, the criteria were clustered according to product, material, and production-related factors and depicted in three-dimensional suitability diagrams. Therefore, a weighted average was calculated using the respective weighting factors for each category.

In a third step, the technology readiness of the most promising technologies was evaluated by the same experts based on the method introduced by Reinhart et al. (2012)[109]. Technology readiness in this context means the technical and economic understanding and achievable performance of a technology in the current state of development for a certain purpose of operation in manufacturing. Schindler (2015)[110] therefore introduced questionnaires to structurally gather information about the development state of a technology clustered by seven technology readiness levels (TRL) similar to the NASA TRL approach[111], which was adapted towards the evaluation of production technologies. The scale starts with level 1, the basic research level, where fundamental physical relations and process parameters need to be understood and fields of application need to be identified. In level 2, the feasibility study, the theoretical understanding of level 1 is validated in simple experiments or simulations. Level 3, the technology development level, focusses on the development of a conceptual application as basis for a prototype, which is designed in level 4. The aim of a level 4 prototype is the validation of process parameters and technology functions. Level 5 comprises the integration of the technology in an operating resource like a machine tool inside a laboratory environment but under real-life conditions. Within this level,

first performance figures are determined. In level 6, the production structure level, the technology is integrated into the production structure with preceding and subsequent technologies in order to identify real-life performance and interdependencies with the other technologies. Level 7 describes the serial application phase, where the industrial production performance is optimized and processes are standardized. An exemplary questionnaire (translated to English) adapted to ASSB layer fabrication can be found in Supplementary Figures S1-S7.

In order to take into account information uncertainty, each question or criterion was extended by the level of information uncertainty. Especially in early development stages or innovative application cases of a technology, information about technical or economic performance may be unknown or uncertain but can be estimated based on experiences from other applications[109]. These uncertainties were included by carrying out a Monte-Carlo Simulation for each question or criterion. Dependent on the level of uncertainty, deviation corridors of the made assumptions were defined and modeled as a Gaussian standard distribution. The Monte-Carlo Simulation generates a random value within this corridor following the probability distribution for each simulation run. The values of each simulation run for each question or criterion were added up, weighted by the defined importance of each question or criterion and the weight of the subordinate TRL, which leads to a technology readiness index. Supplementary Figure S8 shows an exemplary evaluation of the technology readiness by levels 1-7, whereas the histograms derived by Monte-Carlo-Simulation are depicted in Figure 2 (image c).

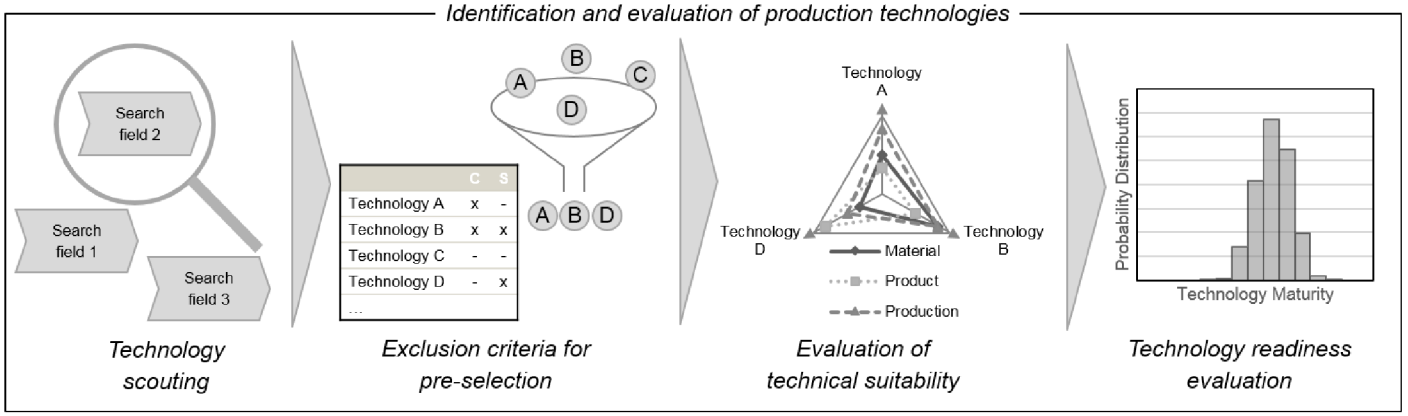

Figure 5: Method for technology identification and evaluation. After technology scouting[108], technologies are pre-selected and evaluated with regard to technical suitability[69]. Finally, the maturity of the selected technologies is analyzed[109].

Cost modeling

A top down calculation was carried through to estimate production cost for an oxide based ASSB produced in small scale and large scale. The base case scenario for cost modeling is a 100 x 100 mm² SOFC with a 90 µm thick electrolyte produced by tape casting and sintering (1300-1500 °C), as well as 30 µm thick electrodes manufactured by subsequent screen printing and co-sintering (1000-1200 °C). A hybrid electric vehicle (HEV) standard format[103] (DIN 91252: 85 x 120 mm²; taking into account 1 mm (corresponding to 0.5 mm wall thickness) for housing and isolation results in an area of 84 x 119 mm²) was assumed for the ASSB, corresponding to the same area as for the Kerafol SOFC. A 70 µm thick high-voltage spinel $LiNi_{0.5}Mn_{1.5}O_4$ (LNMO, 140 mAh/g, 4.7 V)[97] composite cathode with 30 vol% LLZ, 5 vol% PVdF, and 5 vol% carbon black was assumed as base case scenario. According to the considerations presented in section 2.1, the thickness of the LLZ separator layer was set to 10 µm, hypothesizing that a layer with these dimensions can be economically fabricated. The dimensions of the composite anode (incl. 30 vol% LLZ) were calculated based on the area specific capacity of the cathode (2.6 mAh/cm²), with a 10 % excess anode capacity. Given that the cathode is already in a lithiated state, sufficient "free" space needs to be taken into account for the lithium to be plated during the first charge, while only the surplus of lithium needs to be considered for the cost calculation. Finally, a 10 µm thick bipolar aluminum current collector with a thin copper layer (1 vol%) on the anode side was assumed. Note that additional material cost could occur when taking into account costs for solvents, sintering aids, pore formers, etc. Further calculated scenarios (cf. Table 3) also include Ni- and Li-rich $LiNi_{1-x-y}Mn_xCo_yO_2$ (NMC811, 200 mAh/g, 3.7 V; HE-NMC, 300 mAh/g, 3.4 V)[100,112].

For fabrication of the cell stack and housing, additional costs need to be taken into account. According to Kerafol, the processing cost per SOFC stack C_{stack} can be roughly estimated as the processing cost per galvanic cell C_{cell} multiplied by the number of galvanic cells n and a factor of two to account for the assembly process:

$$C_{stack} = 2 \cdot n \cdot C_{cell} \quad (2)$$

The processing cost $C(N)$ was calculated as

$$C(N) = C_{stack} \cdot N^{\frac{\log(1-\alpha)}{\log 2}}, (3)$$

where N is the cumulative number of stacks produced and α represents the learning rate[113]. Estimated learning rates for EV

battery packs[107] range from 6-9 %[114] to 16±4 %[102], while learning rates of 16-17 % were estimated for EV battery cells[115] and up to 30±3 % for lithium-ion cells in electronics[102]. Resulting costs for different scenarios can be found in Table 3.

Conflicts of interest

There are no conflicts to declare.

Acknowledgements

We sincerely thank the Federal Ministry for Education and Research (Bundesministerium für Bildung und Forschung) for financial support. The results presented in this paper have been compiled in the frame of the project "FELIZIA" (grant numbers 03XP0026E and 03XP0026I). We would also like to thank the company Kerafol Keramische Folien GmbH and Franz-Martin Fuchs for providing estimations for SOFC manufacturing cost and the company MSE Supplies LLC for estimation of the LLZ price. We would like to thank Georg Mauer for his valuable input concerning the technology evaluation and Till Günther for proof-reading of the manuscript.

References

1. A. Mauger and C. M. Julien, *Ionics*, 2017, **23**(8), 1933.
2. Y.-S. Hu, *Nat. Energy*, 2016, **1**(4), 16042.
3. L. Yue, J. Ma, J. Zhang, J. Zhao, S. Dong, Z. Liu, G. Cui and L. Chen, *Energy Storage Materials*, 2016, **5**, 139.
4. H. Muramatsu, A. Hayashi, T. Ohtomo, S. Hama and M. Tatsumisago, *Solid State Ionics*, 2011, **182**(1), 116.
5. Y. Ren, K. Chen, R. Chen, T. Liu, Y. Zhang, C.-W. Nan and B. Vyas, *J. Am. Ceram. Soc.*, 2015, **98**(12), 3603.
6. J. Janek and W. G. Zeier, *Nat. Energy*, 2016, **1**(9), 16141.
7. T. Placke, R. Kloepsch, S. Dühnen and M. Winter, *J Solid State Electrochem*, 2017, **21**(7), 1939.
8. C.-L. Tsai, V. Roddatis, C. V. Chandran, Q. Ma, S. Uhlenbruck, M. Bram, P. Heitjans and O. Guillon, *ACS applied materials & interfaces*, 2016, **8**(16), 10617.
9. X. Han, Y. Gong, K. K. Fu, X. He, G. T. Hitz, J. Dai, A. Pearse, B. Liu, H. Wang, G. Rubloff, Y. Mo, V. Thangadurai, E. D. Wachsman and L. Hu, *Nature materials*, 2016.
10. Y. Li, J.-T. Han, C.-A. Wang, H. Xie and J. B. Goodenough, *J. Mater. Chem.*, 2012, **22**(30), 15357.
11. L. Cheng, J. S. Park, H. Hou, V. Zorba, G. Chen, T. Richardson, J. Cabana, R. Russo and M. Doeff, *J. Mater. Chem. A*, 2014, **2**(1), 172.
12. J.-M. Tarascon and M. Armand, *Nature*, 2001, **414**, 359 EP -.
13. S. Ohta, J. Seki, Y. Yagi, Y. Kihira, T. Tani and T. Asaoka, *Journal of Power Sources*, 2014, **265**, 40.
14. J. Schnell, A. Hofer, C. Singer, T. Günther and G. Reinhart in *7. WGP-Jahreskongress Aachen: Aachen, 5.-6. Oktober 2017*, ed. R. Schmitt and G. Schuh, Apprimus Verlag, Aachen, 2017, p 295.
15. J. Schnell, T. Günther, T. Knoche, C. Vieider, L. Köhler, A. Just, M. Keller, S. Passerini and G. Reinhart, *Journal of Power Sources*, 2018, **382**, 160.
16. A. Manuel Stephan and K. S. Nahm, *Polymer*, 2006, **47**(16), 5952.
17. Y. Zhu, X. He and Y. Mo, *ACS applied materials & interfaces*, 2015, **7**(42), 23685.
18. Y. Kato, S. Shiotani, K. Morita, K. Suzuki, M. Hirayama and R. Kanno, *The journal of physical chemistry letters*, 2018, **9**(3), 607.
19. A. Sakuda, A. Hayashi and M. Tatsumisago, *Scientific reports*, 2013, **3**, 2261.
20. T. Liu, Y. Zhang, R. Chen, S.-X. Zhao, Y. Lin, C.-W. Nan and Y. Shen, *Electrochemistry Communications*, 2017, **79**, 1.
21. S. Troy, A. Schreiber, T. Reppert, H.-G. Gehrke, M. Finsterbusch, S. Uhlenbruck and P. Stenzel, *Applied Energy*, 2016, **169**, 757.
22. D. Andre, S.-J. Kim, P. Lamp, S. F. Lux, F. Maglia, O. Paschos and B. Stiaszny, *J. Mater. Chem. A*, 2015, **3**(13), 6709.
23. J. Li, C. Ma, M. Chi, C. Liang and N. J. Dudney, *Adv. Energy Mater.*, 2015, **5**(4), 1401408.
24. K. Kerman, A. Luntz, V. Viswanathan, Y.-M. Chiang and Z. Chen, *J. Electrochem. Soc.*, 2017, **164**(7), A1731-A1744.
25. P.E. Stallworth, J.J. Fontanella, M.C. Wintersgill, C. D. Scheidler, J. J. Immel, S.G. Greenbaum and A.S. Gozdz, *Journal of Power Sources*, 1999, **81-82**, 739.
26. https://www.smartgrid.gov/files/Seeo_SolidStateBatteries_FTR_DE-OE0000223_0.pdf (last accessed October 2016).
27. http://www.bluecar.fr/les-batteries-lmp-lithium-metal-polymere (last accessed August 2018).
28. B. C. H. Steele, *Journal of Materials Science*, 2001, **36**(5), 1053.
29. https://separators.freudenberg-pm.com/products (last accessed August 2018).
30. R. B. MacMullin and G. A. Muccini, *AIChE J.*, 1956, **2**(3), 393.
31. C.-L. Tsai, E. Dashjav, E.-M. Hammer, M. Finsterbusch, F. Tietz, S. Uhlenbruck and H. P. Buchkremer, *J Electroceram*, 2015, **35**(1-4), 25.
32. H. Duan, H. Zheng, Y. Zhou, B. Xu and H. Liu, *Solid State Ionics*, 2018, **318**, 45.
33. F. Han, Y. Zhu, X. He, Y. Mo and C. Wang, *Adv. Energy Mater.*, 2016, **6**(8), 1501590.
34. N. Kamaya, K. Homma, Y. Yamakawa, M. Hirayama, R. Kanno, M. Yonemura, T. Kamiyama, Y. Kato, S. Hama, K. Kawamoto and A. Mitsui, *Nature materials*, 2011, **10**(9), 682.
35. R. Kanno and Masahiro Murayama, *J. Electrochem. Soc.*, 2001, **148**(7), A742-A746.
36. P. Bron, S. Johansson, K. Zick, J. Schmedt auf der Günne, S. Dehnen and B. Roling, *Journal of the American Chemical Society*, 2013, **135**(42), 15694.
37. P. Bron, S. Dehnen and B. Roling, *Journal of Power Sources*, 2016, **329**, 530.
38. Y. Kato, S. Hori, T. Saito, K. Suzuki, M. Hirayama, A. Mitsui, M. Yonemura, H. Iba and R. Kanno, *Nat. Energy*, 2016, **1**(4), 16030.
39. Y. Seino, T. Ota, K. Takada, A. Hayashi and M. Tatsumisago, *Energy Environ. Sci.*, 2014, **7**(2), 627.
40. R. Murugan, V. Thangadurai and W. Weppner, *Angewandte Chemie (International ed. in English)*, 2007, **46**(41), 7778.
41. Y. Inaguma, C. Liquan, M. Itoh, T. Nakamura, T. Uchida, H. Ikuta and M. Wakihara, *Solid State Communications*, 1993, **86**(10), 689.
42. H. Aono, *J. Electrochem. Soc.*, 1989, **136**(2), 590.
43. Q. Ma, Q. Xu, C.-L. Tsai, F. Tietz, O. Guillon and B. Dunn, *J. Am. Ceram. Soc.*, 2016, **99**(2), 410.
44. W. H. Meyer, *Adv. Mater.*, 1998, **10**(6), 439.
45. L. Edman, A. Ferry and M. M. Doeff, *J. Mater. Res.*, 2000, **15**(09), 1950.
46. D. Lin, W. Liu, Y. Liu, H. R. Lee, P.-C. Hsu, K. Liu and Y. Cui, *Nano letters*, 2016, **16**(1), 459.
47. E. D. Wachsman, L. Hu and V. Thangadurai, *Ion conducting batteries with solid state electrolyte materials*(US20140287305 A1), Google Patents, 2014. https://www.google.com/patents/US20140287305.
48. Y. J. Nam, D. Y. Oh, S. H. Jung and Y. S. Jung, *Journal of Power Sources*, 2018, **375**, 93.
49. W. G. Coors, J. H. Gordon and S. G. Menzer, *Electrochemical cell comprising ionically conductive membrane and porous multiphase electrode*(US20100297537A1), 2010. https://patents.google.com/patent/US20100297537A1/en?oq=US+patent+application+2010%2f0297537+A1 (last accessed June 2018).
50. K. Wincewicz and J. Cooper, *Journal of Power Sources*, 2005, **140**(2), 280.
51. T. Kato, R. Yoshida, K. Yamamoto, T. Hirayama, M. Motoyama, W. C. West and Y. Iriyama, *Journal of Power Sources*, 2016, **325**, 584.
52. L. Miara, A. Windmüller, C.-L. Tsai, W. D. Richards, Q. Ma, S. Uhlenbruck, O. Guillon and G. Ceder, *ACS applied materials & interfaces*, 2016, **8**(40), 26842.
53. M. Gellert, E. Dashjav, D. Grüner, Q. Ma and F. Tietz, *Ionics*, 2018, **24**(4), 1001.

54. D. Wang, Q. Sun, J. Luo, J. Liang, Y. Sun, R. Li, K. Adair, L. Zhang, R. Yang, S. Lu, H. Huang and X. Sun, *ACS applied materials & interfaces*, 2019, **11**(5), 4954.
55. E. Yi, W. Wang, J. Kieffer and R. M. Laine, *Journal of Power Sources*, 2017, **352**, 156.
56. S. McIntosh and R. J. Gorte, *Chem. Rev.*, 2004, **104**(10), 4845.
57. R. J. Gorte and J. M. Vohs, *Current Opinion in Colloid & Interface Science*, 2009, **14**(4), 236.
58. C. Yang, L. Zhang, B. Liu, S. Xu, T. Hamann, D. McOwen, J. Dai, W. Luo, Y. Gong, E. D. Wachsman and L. Hu, *Proceedings of the National Academy of Sciences of the United States of America*, 2018, **115**(15), 3770.
59. G. T. Hitz, D. W. McOwen, L. Zhang, Z. Ma, Z. Fu, Y. Wen, Y. Gong, J. Dai, T. R. Hamann, L. Hu and E. D. Wachsman, *Materials Today*, 2019, **22**, 50.
60. M. Shoji, H. Munakata and K. Kanamura, *Front. Energy Res.*, 2016, **4**, 590.
61. J. B. Habedank, J. Endres, P. Schmitz, M. F. Zaeh and H. P. Huber, *Journal of Laser Applications*, 2018, **30**(3), 32205.
62. A. Patil, V. Patil, D. Wook Shin, J.-W. Choi, D.-S. Paik and S.-J. Yoon, *Materials Research Bulletin*, 2008, **43**(8-9), 1913.
63. C.-W. Ahn, J.-J. Choi, J. Ryu, B.-D. Hahn, J.-W. Kim, W.-H. Yoon, J.-H. Choi and D.-S. Park, *Journal of the Electrochemical Society*, 2014, **162**(1), A60-A63.
64. D. Hanft, J. Exner and R. Moos, *Journal of Power Sources*, 2017, **361**, 61.
65. F. Tietz, H.-P. Buchkremer and D. Stöver, *Solid State Ionics*, 2002, **152-153**, 373.
66. N. H. Menzler, J. Malzbender, P. Schoderböck, R. Kauert and H. P. Buchkremer, *Fuel Cells*, 2014, **14**(1), 96.
67. R. N. Basu, G. Blass, H. P. Buchkremer, D. Stöver, F. Tietz, E. Wessel and I. C. Vinke, *Journal of the European Ceramic Society*, 2005, **25**(4), 463.
68. M.-J. Pan and C. A. Randall, *IEEE Electr. Insul. Mag.*, 2010, **26**(3), 44.
69. F. Klocke, M. Fallböhmer, A. Kopner and G. Trommer, *Robotics and Computer-Integrated Manufacturing*, 2000, **16**(6), 411.
70. S.-W. Baek, J.-M. Lee, T. Y. Kim, M.-S. Song and Y. Park, *Journal of Power Sources*, 2014, **249**, 197.
71. T. Kato, S. Iwasaki, Y. Ishii, M. Motoyama, W. C. West, Y. Yamamoto and Y. Iriyama, *Journal of Power Sources*, 2016, **303**, 65.
72. Y. Ren, T. Liu, Y. Shen, Y. Lin and C.-W. Nan, *Ionics*, 2017, **23**(9), 2521.
73. S. Xu, D. W. McOwen, L. Zhang, G. T. Hitz, C. Wang, Z. Ma, C. Chen, W. Luo, J. Dai, Y. Kuang, E. M. Hitz, K. Fu, Y. Gong, E. D. Wachsman and L. Hu, *Energy Storage Materials*, 2018, **15**, 458.
74. J. Schnell and G. Reinhart, *Procedia CIRP*, 2016, **57**, 568.
75. W. Xia, B. Xu, H. Duan, X. Tang, Y. Guo, H. Kang, H. Li and H. Liu, *J American Ceramic Society*, 2017, **100**(7), 2832.
76. K. Fu, Y. Gong, G. T. Hitz, D. W. McOwen, Y. Li, S. Xu, Y. Wen, L. Zhang, C. Wang, G. Pastel, J. Dai, B. Liu, H. Xie, Y. Yao, E. D. Wachsman and L. Hu, *Energy Environ. Sci.*, 2017, **10**(7), 1568.
77. S. Xu, D. W. McOwen, C. Wang, L. Zhang, W. Luo, C. Chen, Y. Li, Y. Gong, J. Dai, Y. Kuang, C. Yang, T. R. Hamann, E. D. Wachsman and L. Hu, *Nano letters*, 2018, **18**(6), 3926.
78. N. H. Menzler, F. Tietz, S. Uhlenbruck, H. P. Buchkremer and D. Stöver, *Journal of Materials Science*, 2010, **45**(12), 3109.
79. J. S. Reed, *Principles of ceramics processing*, Wiley, New York, 1995.
80. S. Stolz, W. Bauer, H.-J. Ritzhaupt-Kleissl and J. Haußelt, *Journal of the European Ceramic Society*, 2004, **24**(6), 1087.
81. J. R. Groza, *Materials processing handbook*, Taylor & Francis distributor, Boca Raton, Fla, London, 2007.
82. P. Sarkar and P. S. Nicholson, *Journal of the American Ceramic Society*, **79**(8), 1987.
83. L. Besra and M. Liu, *Progress in Materials Science*, 2007, **52**(1), 1.
84. J. Will, *Solid State Ionics*, 2000, **131**(1-2), 79.
85. U. B. Pal, *J. Electrochem. Soc.*, 1990, **137**(9), 2937.
86. D. M. Mattox, *Handbook of physical vapor deposition (PVD) processing*, William Andrew, Oxford, UK, 2010.
87. J. Akedo, *J American Ceramic Society*, 2006, **89**(6), 1834.
88. J. Iwasawa, R. Nishimizu, M. Tokita, M. Kiyohara and K. Uematsu, *J American Ceramic Society*, 2007, **90**(8), 2327.
89. D.-W. Lee, H.-J. Kim, Y.-H. Kim, Y.-H. Yun and S.-M. Nam, *J American Ceramic Society*, 2011, **94**(9), 3131.
90. D. Hanft, J. Exner, M. Schubert, T. Stöcker, P. Fuierer and R. Moos, *J. Ceram. Sci. Technol*, 2015, **6**(3), 147.
91. C. Zhang, H. L. Liao, W. Y. Li, G. Zhang, C. Coddet, C. J. Li, C. X. Li and X. J. Ning, *Journal of Thermal Spray Technology*, 2006, **15**(4), 598.
92. L. Pawłowski, *The science and engineering of thermal spray coatings*, Wiley, Chichester, England, Hoboken, NJ, 2008.
93. R. B. Heimann, *Plasma-Spray Coating*, Wiley-VCH, Hoboken, 2008.
94. A. Vardelle, C. Moreau, N. J. Themelis and C. Chazelas, *Plasma Chem Plasma Process*, 2015, **35**(3), 491.
95. S. Kuroda, J. Kawakita, M. Watanabe and H. Katanoda, *Science and technology of advanced materials*, 2008, **9**(3), 33002.
96. R. Schmuch, R. Wagner, G. Hörpel, T. Placke and M. Winter, *Nat. Energy*, 2018, **3**(4), 267.
97. E. J. Berg, C. Villevieille, D. Streich, S. Trabesinger and P. Novák, *J. Electrochem. Soc.*, 2015, **162**(14), A2468-A2475.
98. G. Patry, A. Romagny, S. Martinet and D. Froelich, *Energy Sci Eng*, 2015, **3**(1), 71.
99. J.-H. Schünemann, *Modell zur Bewertung der Herstellkosten von Lithiumionenbatteriezellen*, Zugl.: Braunschweig, Techn. Univ., Diss., 2015, Sierke, Göttingen, 2015.
100. B. Qiu, M. Zhang, L. Wu, J. Wang, Y. Xia, D. Qian, H. Liu, S. Hy, Y. Chen, K. An, Y. Zhu, Z. Liu and Y. S. Meng, *Nature communications*, 2016, **7**, 12108.
101. V. Pimenta, M. Sathiya, D. Batuk, A. M. Abakumov, D. Giaume, S. Cassaignon, D. Larcher and J.-M. Tarascon, *Chem. Mater.*, 2017, **29**(23), 9923.
102. O. Schmidt, A. Hawkes, A. Gambhir and I. Staffell, *Nat. Energy*, 2017, **2**(8), 17110.
103. DIN, *Electrically propelled road vehicles – Battery systems – Design specifications for Lithium-Ion battery cells*(91252), Beuth, Berlin, 2016.
104. https://electrek.co/2019/01/12/tesla-gigafactory-1-produced-half-billion-battery-cells/ (last accessed March 2019).
105. R. J. Brodd and C. Helou, *Journal of Power Sources*, 2013, **231**, 293.
106. A. Kwade, W. Haselrieder, R. Leithoff, A. Modlinger, F. Dietrich and K. Droeder, *Nat. Energy*, 2018, **3**(4), 290.
107. B. Nykvist and M. Nilsson, *Nature Clim Change*, 2015, **5**(4), 329.
108. J. Greitemann, M. Hehl, D. Wagner and G. Reinhart, *Prod. Eng. Res. Devel.*, 2016, **10**(3), 337.
109. G. Reinhart, S. Schindler and P. Krebs in *Glocalized Solutions for Sustainability in Manufacturing: Proceedings of the 18th CIRP International Conference on Life Cycle Engineering, Technische Universität Braunschweig, Braunschweig, Germany, May 2nd - 4th, 2011*, ed. J. Hesselbach and C. Herrmann, Springer Berlin Heidelberg, Berlin, Heidelberg, 2011, p 179.
110. S. Schindler, *Strategische Planung von Technologieketten für die Produktion*, Utz, München, 2015.
111. J. C. Mankins, *White Paper, April*, 1995, **6**.
112. H.-J. Noh, S. Youn, C. S. Yoon and Y.-K. Sun, *Journal of Power Sources*, 2013, **233**, 121.
113. L. E. Yelle, *Decision Sciences*, 1979, **10**(2), 302.
114. M. Weiss, M. K. Patel, M. Junginger, A. Perujo, P. Bonnel and G. van Grootveld, *Energy Policy*, 2012, **48**, 374.
115. S. J. Gerssen-Gondelach and A. P.C. Faaij, *Journal of Power Sources*, 2012, **212**, 111.